基于复合双环腔及饱和吸收体的单纵模窄线宽掺铥光纤激光器

高娇[1]，延凤平[1*]，冯亭[2]，杨丹丹[1]，李挺[1]，秦齐[1]，郭浩[1]，谭浩宇[1]，李光波[1]

[1]北京交通大学电子信息工程学院，北京 100044；
[2]光信息技术创新中心，河北大学物理科学与技术学院，河北 保定 071002

摘要 提出并实现了一种工作在2050 nm波段的单纵模窄线宽掺铥光纤激光器。使用3个耦合器组成的新型复合双环腔抑制密集的多纵模，结合未泵浦的掺铥光纤（作为饱和吸收体），实现了激光的单纵模激射和窄线宽输出。实验结果表明：室温下，激光器的中心波长为2048.76 nm，光信噪比为68 dB。通过60 min的连续测量，得到激光的输出功率波动不大于0.15 dB，中心波长漂移不大于0.02 nm，证明了所设计的激光器具有良好的波长稳定性和功率稳定性。使用基于3×3光纤耦合器的相位解调系统对激光器的频率噪声特性进行测量，并进一步结合β分割线法测量线宽。当测量时间为0.001 s时，激光器的线宽为9.17 kHz。当频率高于1 MHz时，相对强度噪声低于-125.69 dB/Hz。该激光器在激光雷达和空间光通信系统中具有广阔的应用前景。

关键词 激光器；掺铥光纤激光器；单纵模；子环腔；饱和吸收体

中图分类号 O436　　　**文献标志码** A　　　　　　　　**DOI:** 10.3788/CJL230525

1 引　　言

掺铥光纤激光器（TDFL）的可调谐范围在1400～2200 nm之间[1]，这一范围涵盖了大气传输窗口。在该窗口中，光在自由空间中允许传输的功率比其他波段高几个数量级。特别地，光在2050 nm附近的功率透射率超过了80%，这使得在自由空间光通信中使用2050 nm波段掺铥光纤激光器成为可能[2]。单纵模（SLM）光纤激光器具有光束质量高、相干性好、线宽窄等优良特性[3]，在很多重要领域被作为首选光源[4]。例如，具有窄线宽输出的光纤激光器已被用于超长距离相干光通信、光纤传感、光学计量、高分辨率光谱和激光雷达等领域[5-9]，而且在光学原子钟等方面也具有潜在的应用前景[10-11]。

目前实现单纵模的方法有滤波法[12]、将选频滤波器结合未泵浦的有源光纤作为饱和吸收体（SA）的方法[13-15]、复合腔法[16-20]等。第一种方法是实现单纵模的常见方法，具有良好的滤波效果，但其使用了超窄带滤波器，而超窄带滤波器的制作成本较高。2013年，李琦等[21]以啁啾Moiré光纤光栅作为超窄带滤波器，实现了激光器的稳定单频运转。第二种方法通过饱和吸收体和各类选频滤波器的共同作用实现对纵模振荡的抑制，实现单纵模运转。2016年，白燕等[22]利用未泵

浦的掺铥光纤结合法布里-珀罗（F-P）滤波器实现了中心波长为1941.6 nm、光信噪比32 dB的单纵模激光输出。2019年，白燕等[23]利用可有效缓解偏振态引起的随机误差以及系统不稳定性的保偏掺铥光纤作为饱和吸收体，结合F-P滤波器在环腔结构中实现了更加稳定的单纵模光纤激光输出。第三种方法使用耦合器制作复合腔，基于游标效应扩展自由光谱范围（FSR，在公式中记为R_{fs}）[24]，利用窄透射带宽实现单纵模输出。2021年，Zhang等[25]利用3个2×2耦合器（OCs）设计了三环复合腔，将其与自制的取样保偏光纤布拉格光栅结合实现了六波长可切换的单纵模激光输出。然而，由于$2~\mu m$波段处的关键滤波器组件相对缺乏且成本较高[20]，加之复合腔的结构较为复杂，该方案对环腔长度及耦合比的设计要求比较严苛，且易受外界环境的影响。鉴于此，笔者考虑采用简单易制的复合双环腔结合可饱和吸收体作为上述方案的替代，以实现更经济稳定的单纵模激光输出。

笔者提出并通过实验验证了一种复合双环腔与一段未泵浦掺铥光纤相结合的单纵模窄线宽掺铥光纤激光器。首先详细介绍了复合双环腔滤波器的设计和制作，通过改变耦合器的耦合比和子腔长度调整滤波器的自由光谱范围和主干涉峰透射带宽。然后，将该结构与两种不同结构参数的双环腔滤波器进行性能对比

分析,结果显示:该复合腔滤波器能够实现良好的滤波效果。最后,简要分析了未泵浦的掺铥光纤(作为饱和吸收体)抑制纵模的原理,并搭建了环腔掺铥光纤激光器,测量结果表明:在室温下,该激光器的输出中心波长为 2048.76 nm,光信噪比为 68 dB。采用基于 3×3 耦合器的非平衡迈克耳孙干涉仪和相位信号解调的线宽测量系统对激光器的频率噪声特性进行测量,使用 β-分割线法对所设计的激光器进行线宽分析计算,结果表明:当测量时间为 0.001 s 时,输出激光线宽为 9.17 kHz;当频率高于 1 MHz 时,相对强度噪声低于 −125.69 dB/Hz。

2 实验装置

2.1 实验结构

图 1 为搭建的基于复合双环腔与饱和吸收体的单纵模掺铥光纤激光器的结构示意图,该结构主要由环形主腔与复合子腔组成。

将 793 nm 泵浦源输出通过(2＋1)×1 的光纤合束器(FC)输入到环腔中,采用 4 m 长的双包层掺铥光纤(TDF,Nufern SM-TDF-10P/130M)作为增益介质,环形器保证环腔内光的单向传输。环形器的端口 2 加入长度为 0.5 m 的未泵浦的掺铥光纤作为饱和吸收体,使其等效于一种动态自追踪窄带滤波器,以有效抑制多纵模振荡,实现单纵模运转并压窄线宽。光纤布拉格光栅(FBG)作为波长选择器件[26],其中心波长为 2048.76 nm,3 dB 带宽为 0.13 nm,透射谱如图 2 所示。经光纤布拉格光栅反射后的光信号注入到由 3 个耦合器组成的复合双环腔中,进行下一步的模式挑选。输出激光由 90:10 耦合器的 10% 端口输出。激光器的腔长为 18 m,对应纵模间隔为 11.5 MHz。
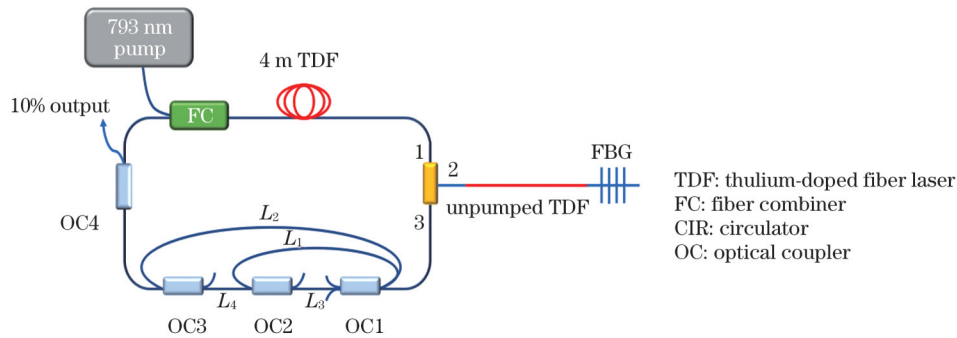

图 1 单纵模光纤激光器的结构示意图

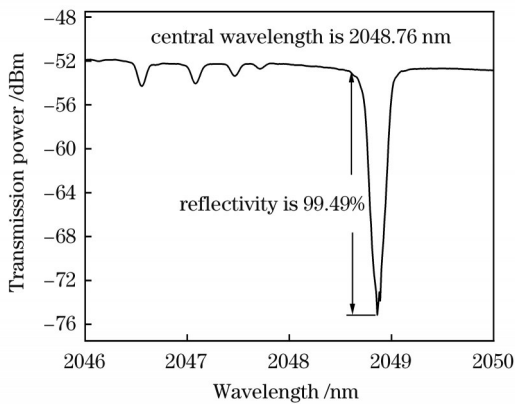Fig. 1 Structure diagram of SLM fiber laser

图 2 光纤布拉格光栅的透射谱

Fig. 2 Transmission spectrum of FBG

2.2 复合双环腔结构及选频特性的仿真分析

复合双环腔结构如图 3 所示,由 1 个 3×3 耦合器(OC1)和 2 个 2×2 耦合器(1 个 OC2 和 1 个 OC3)依次连接而成。3×3 耦合器 OC1 为 33:33:33 输出,分成三路光信号;2 个 2×2 耦合器的耦合比均为 20:80。设输入光场 $E_{in}=E_1$,将激光腔内各个端口的连接光纤分别标号为 L_1、L_2、L_3、L_4,各段光纤长度分别为 $l_1=2.35$ m,$l_2=1.31$ m,$l_3=1$ m,$l_4=1$ m。L_1-L_3 与 L_2-L_3-L_4 形成了两个闭合的谐振环,两闭合谐振环长度分别为 3.35 m

与 3.31 m,对应的自由光谱范围为 61.8 MHz 和 62.6 MHz。由于光场之间是独立的,最终的输出光是由直通耦合的输出场与环腔振荡耦合的输出场叠加而成的,通过 OC3 的端口 13 输出。两闭合谐振环长度相差 $\Delta l(\Delta l=4$ cm),根据游标效应,当两个谐振环的长度比较接近时,复合双环腔滤波器的自由光谱范围 $R_{fs}=\dfrac{c}{n_{eff}\Delta l}=5.18$ GHz(≈0.072 nm),其中:n_{eff} 为有效折射率,在 2 μm 波段下有效折射率为 1.447;c 为光速。由此可知,两个单环组合而成的复合腔可用来形成干涉,增大自由光谱范围。
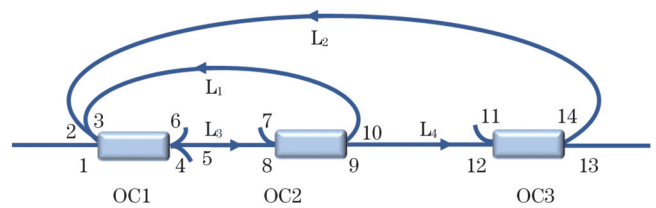

图 3 子环腔结构图

Fig. 3 Structure diagram of subring cavity

下面分析复合双环腔的滤波特性。使用子环腔进行滤波时需要严格满足以下两个条件[25]:

1) 复合双环腔形成的自由光谱范围是光纤布拉

格光栅反射带宽的 50%~100%；

2）复合双环腔的有效传输通带主谐振峰带宽是主腔纵模间隔的 1~2 倍。

由复合双环腔的结构分析可知复合腔滤波器的自由光谱范围为 5.18 GHz（≈0.072 nm），光纤布拉格光栅的 3 dB 带宽为 0.13 nm，满足条件 1）。激光器的腔内纵模间隔为 11.5 MHz，所以子环腔主干涉峰的 3 dB 带宽要小于 23 MHz。而主干涉峰带宽由复合腔中较长的闭合谐振环的长度决定，根据子环腔干涉峰带宽公式 $\Delta v = \dfrac{c\delta}{2\pi n_{\mathrm{eff}}(l_1+l_3)}$ 计算得到此干涉峰带宽为 13.6 MHz[27]，满足条件 2）。δ 为光在子环腔中传输一圈后的传输损耗，由公式 $\delta = \ln(I_0/I_1)$ 得到，其中 I_0 为输入光强，I_1 为传输一周后的光强。

基于子环腔滤波器的分析方法[28]，由耦合器的传输矩阵理论可以得到各个端口的光强为

$$\begin{bmatrix} E_4 \\ E_5 \\ E_6 \end{bmatrix} = \frac{1}{\sqrt{3}} \begin{bmatrix} 1 & \exp\left(\dfrac{2\pi j}{3}\right) & \exp\left(\dfrac{2\pi j}{3}\right) \\ \exp\left(\dfrac{2\pi j}{3}\right) & 1 & \exp\left(\dfrac{2\pi j}{3}\right) \\ \exp\left(\dfrac{2\pi j}{3}\right) & \exp\left(\dfrac{2\pi j}{3}\right) & 1 \end{bmatrix} \begin{bmatrix} E_1 \\ E_2 \\ E_3 \end{bmatrix}, \tag{1}$$

$$E_8 = E_5 \cdot \sqrt{1-\delta}\, \exp\left[(-\alpha + jk)l_3\right], \tag{2}$$

$$\begin{bmatrix} E_9 \\ E_{10} \end{bmatrix} = \begin{bmatrix} j\sqrt{1-\gamma}\,\sqrt{k_1} & \sqrt{1-\gamma}\,\sqrt{1-k_1} \\ \sqrt{1-\gamma}\,\sqrt{1-k_1} & j\sqrt{1-\gamma}\,\sqrt{k_1} \end{bmatrix} \begin{bmatrix} 0 \\ E_8 \end{bmatrix}, \tag{3}$$

$$E_{12} = E_9 \cdot \sqrt{1-\delta}\, \exp\left[(-\alpha + jk)l_4\right], \tag{4}$$

$$\begin{bmatrix} E_{13} \\ E_{14} \end{bmatrix} = \begin{bmatrix} j\sqrt{1-\gamma}\,\sqrt{k_2} & \sqrt{1-\gamma}\,\sqrt{1-k_2} \\ \sqrt{1-\gamma}\,\sqrt{1-k_2} & j\sqrt{1-\gamma}\,\sqrt{k_2} \end{bmatrix} \begin{bmatrix} 0 \\ E_{12} \end{bmatrix}, \tag{5}$$

$$E_2 = E_{14} \cdot \sqrt{1-\delta}\, \exp\left[(-\alpha + jk)l_2\right], \tag{6}$$

$$E_3 = E_{10} \cdot \sqrt{1-\delta}\, \exp\left[(-\alpha + jk)l_1\right], \tag{7}$$

式中：l_1、l_2、l_3、l_4 为光纤长度；γ 为耦合器的插入损耗；k_i 为第 i 个耦合器的耦合比；α 为光纤损耗系数；δ 为熔接损耗；k 为传输常数；j 表示虚部。根据方程组可以解出该滤波器的场强透射率为

$$E_{13} = \frac{(1-\gamma)^{\frac{3}{2}}\sqrt{1-k_1}\,\sqrt{1-k_2}\,(1-\delta)\exp\left[\dfrac{2\pi j}{3} + (-\alpha+jk)(l_3+l_4)\right]}{\sqrt{3} - j(1-\delta)(1-\gamma)\sqrt{k_1}\exp\left[\dfrac{2\pi j}{3} + (-\alpha+jk)(l_1+l_3)\right] - j(1-\gamma)\sqrt{1-k_1}\,\sqrt{k_2}\,(1-\delta)^{\frac{3}{2}}\exp\left[(-\alpha+jk)(l_2+l_3+l_4)\right]}, \tag{8}$$

复合腔的总透射率为

$$T = \left(\frac{E_{\mathrm{out}}}{E_{\mathrm{in}}}\right)\left(\frac{E_{\mathrm{out}}}{E_{\mathrm{in}}}\right)^* = \left(\frac{E_{13}}{E_1}\right)\left(\frac{E_{13}}{E_1}\right)^* = (E_{13})(E_{13})^*。 \tag{9}$$

根据以上公式进行仿真，得到了该复合腔的透射谱，如图 4 所示。从图 4 可以看出：复合腔的自由光谱范围为 0.07 nm（≈4.99 GHz），与计算结果基本吻合，且大于光纤布拉格光栅反射带宽的 0.5 倍，可以保证在光纤布拉格光栅反射带宽内只有一条有效传输通带[29]；主峰 3 dB 带宽为 14.27 MHz，其值也与计算结果相符，同时也小于主腔纵模间隔的 2 倍，可以实现单纵模选取。

为证明该结构简单易制并且在一定范围内对耦合比及臂长的改变具有容差性，接下来进行参数变化的对比仿真研究。保持两子环长度的差值为 4 cm 不变，在一定范围内改变耦合比和环腔长度，观察其滤波性能的变化。图 5 是 3×3 耦合器 OC1 耦合比为 33∶33∶33、2 个 2×2 耦合器 OC2 和 OC3 的耦合比均为 50∶50 时，两子环 L₁-L₃、L₂-L₃-L₄ 的长度分别为 2 m 和 1.96 m 情况下得到的透射谱示意图。由图 5 可以看出，自由光谱范围与之前的结果保持一致，3 dB 带宽为 14.9 MHz，略微变大，但仍严格满足两个必要条件。通过多次改变参数进行仿真分析，得到了以下结论：设计环长差在 1~5 cm 范围内，耦合比在 50∶50~95∶5 之间，均能满
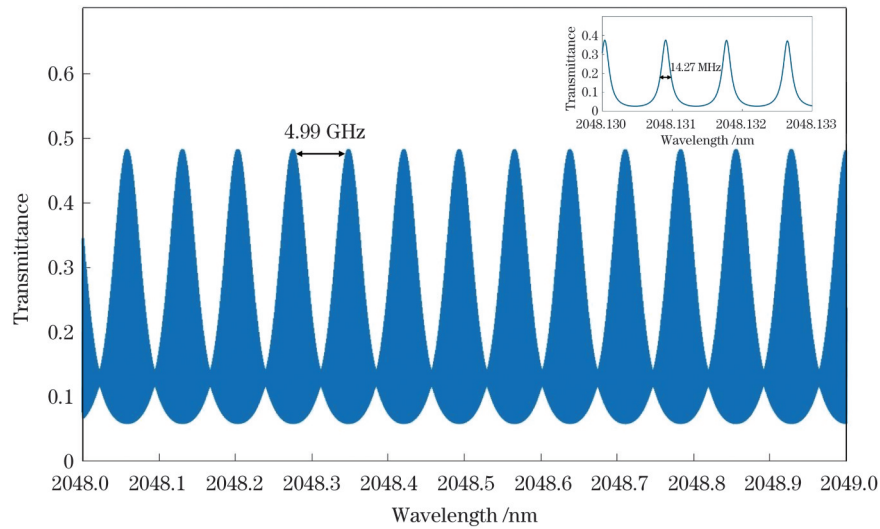
图 4 复合腔滤波器输出的透射谱,插图是激光中心波长处复合腔滤波器透射谱的局部放大

Fig. 4 Transmission spectrum of the proposed compound cavity filter, and the inset is the zoomed-in transmission spectrum of compound cavity filter at the central lasing wavelength
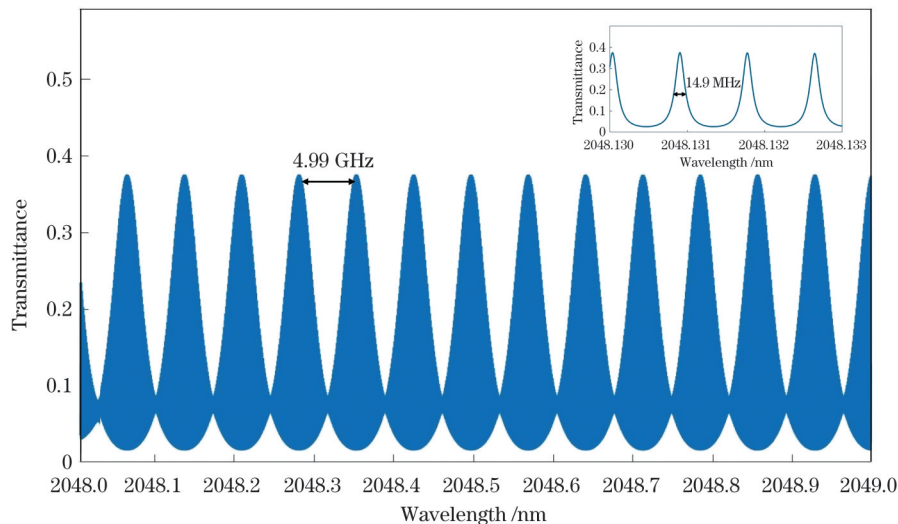

图 5 耦合比为 50:50 的复合腔滤波器的输出透射谱,插图是激光中心波长处复合腔滤波器透射谱的局部放大图

Fig. 5 Transmission spectrum of the proposed compound cavity filter with 50: 50 coupler radio, and the inset is the zoomed-in transmission spectrum of compound cavity filter at the central lasing wavelength

足初步滤波的理论条件,充分证明了该结构具有易于制作、容差性强的特点。

将该结构与 3 个 2×2 耦合器组合成的级联双环腔的滤波性能进行对比分析。级联双环腔的结构如图 6(a)所示,输入光由 OC1 的端口 1 输入,经过 L₁-L₃ 和 L₂ 形成的两个闭合子环依次滤波后由 OC3 的端口 11 输出。滤波器输出透射谱如图 6(b)所示,插图是激光中心波长处双环腔滤波器透射谱的局部放大图。

为了更加准确地对比,依然选择两个子环的长度相差 4 cm,OC1、OC2 和 OC3 的耦合比均选择 80:20。腔内连接光纤 L₁、L₂、L₃、L₄ 的长度分别为 $l_1=1.4$ m,$l_2=1.4$ m,$l_3=0.04$ m,$l_4=0.5$ m,L₁-L₃ 与 L₂ 形成的两个闭合的谐振环的长度分别为 1.44 m 与 1.4 m,得到对应的自由光谱范围依然为 4.99 GHz,而且滤波器滤波光

谱的仿真带宽为 14.27 MHz,虽然也可以满足上述两个条件,但对于图 6(b)所述的透射谱来说,主干涉峰附近存在多个透射率完全相同的干涉峰,无法克服强烈的纵模竞争,滤波性能相对较弱,不能满足所需要求。

2.3 饱和吸收体的工作原理及纵模抑制原理

实验中,选取一段未抽运的掺铥光纤作为饱和吸收体。这段掺铥光纤对非中心频率处的光会产生强烈的吸收,使得激光腔中只剩下中心频率振荡,产生空间烧孔效应,从而使中心频率的光形成单纵模振荡输出。这时的饱和吸收体等效于一种动态自追踪窄带滤波器,可对纵模振荡进行抑制[25]。饱和吸收体的基本结构如图 7 所示。

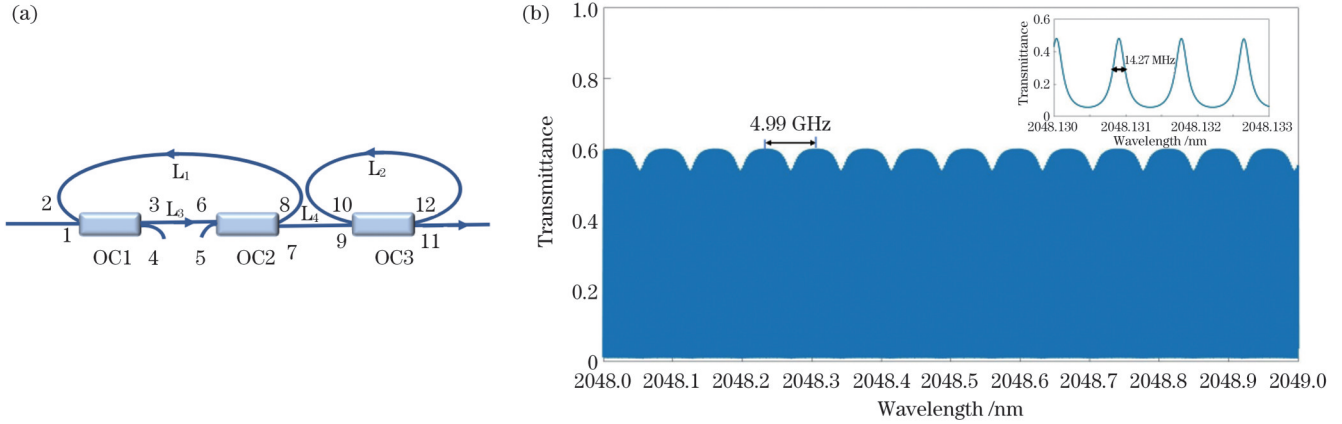饱和吸收体的反射率由前向传输时输出的归一化主纵模的振幅 E_m^+ 与后向传输的纵模振幅 E_m^- 决定:

图 6 级联双环腔结构及其滤波性能。(a) 级联双环腔结构图；(b) 级联双环腔滤波器的输出透射谱，插图是激光中心波长处双环腔滤波器透射谱的局部放大图

Fig.6 Structure and filtering performance of the cascaded double-ring cavity. (a) Schematic of the cascaded double-ring cavity; (b) transmission spectrum of the cascaded double-ring cavity filter, and the inset is the zoomed-in transmission spectrum of the cascaded double-ring cavity filter at the central lasing wavelength
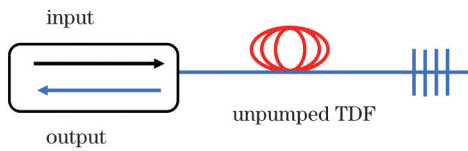

图 7 饱和吸收体的基本结构图

Fig. 7 Fundamental schematic of saturable absorber

$R_e = \left| E_m^- / E_m^+ \right|^2$。饱和吸收体中形成的动态自追踪窄带光栅的带宽表达式为

$$\Delta f = \frac{c}{\lambda} \frac{2\Delta n}{n_{\text{eff}} \lambda} \sqrt{\left(\frac{\Delta n}{2n_{\text{eff}}}\right)^2 + \left(\frac{\lambda}{2n_{\text{eff}} L_{\text{SA}}}\right)^2}, \quad (10)$$

式中：λ 为光栅在最大反射处的中心波长；Δn 为折射率的周期性空间变化，可通过 Kramers-Kronig 关系得出[23]；n_{eff} 为有效折射率；L_{SA} 是饱和吸收体的长度。过长的饱和吸收体会产生强吸收，进而降低光谱的输出功率。在该结构中，已经由自制复合腔对腔内纵模进行初步滤波，腔内剩余的纵模较少，无须加入过长的掺铥光纤。实验中选取长度为 0.5 m 的饱和吸收体连接

于环形器端口 2 的单模尾纤和光纤光栅之间，形成的动态增益光栅可以滤除激光腔内剩余的少量纵模，确保稳定的单纵模输出。

3 实验结果分析与讨论

室温下，在超稳光学平台上搭建激光器并进行测试。当抽运功率达到 4 W 时，可以得到稳定的激光输出。使用分辨率为 0.05 nm 的光谱仪 OSA（YOKOGAWA，AQ6375B）对输出激光进行测量，输出光谱如图 8(a) 所示。中心波长为 2048.76 nm，光信噪比（OSNR）约为 68 dB。在 60 min 内，每隔 6 min 对输出光谱进行一次测量，连续扫描 10 次后得到的光谱如图 8(a) 中的插图所示。为了进一步量化激光器的稳定性，保持泵浦功率不变，对 60 min 内的功率抖动和波长漂移结果进行分析。如图 8(b) 所示，功率波动不大于 0.15 dB，波长漂移不大于 0.02 nm。这一结果表明该激光器在室温下具有良好的输出稳定性。
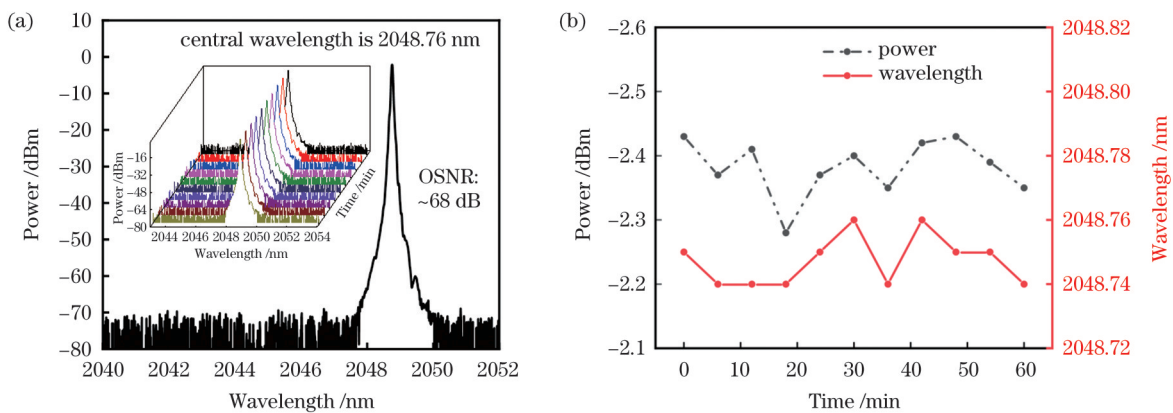
通过自零差法对输出激光的单纵模特性进行检

图 8 激光的输出特性。(a)输出光谱图；(b) 60 min 内波长与功率的波动情况

Fig.8 Output characteristics of the laser. (a) Spectrum of the laser output; (b) wavelength and power fluctuation of the output lasing within 60 min

测。将激光器的输出端口连接到光电探测器(PD)上，将光信号转换为电信号后再接至信号分析仪(Keysight，N9020A)测量输出的射频频谱。设定信号分析仪的扫描范围分别为 0～100 MHz、0～500 MHz和 0～1 GHz，结果分别如图 9(a)、(b)、(c)所示。可见，在上述 3 个测量范围内无明显的跳模现象。为了证明激光器单纵模的稳定性，在 60 min 内对其进行了 10组测量，仍未捕捉到纵模产生的拍频信号，如图 9(a)中的插图所示。通过轻敲实验平台等手法扰动外部环境，也几乎无明显的由纵模拍频产生的频率峰，这表明该激光器运行在稳定的单纵模状态，且不易受外界环境的影响。当去除饱和吸收体后，在 0～500 MHz测量范围内出现了非零频频率峰，如图 9(d)所示。结果表

明，复合双环腔能够较好地抑制腔内的大多数纵模，但腔内的剩余纵模需使用饱和吸收体进一步抑制。

激光在 2048.76 nm 时的相对强度噪声谱由 12.5 GHz的光电探测器、示波器(Tektronix，DPO7104)和信号分析仪在 0～5 MHz 频率范围内测量得到，分辨率带宽(RBW)为 10 kHz。如图 9(e)所示，所提掺铥光纤激光器的相对强度噪声在频率超过 1 MHz 时低于−125.69 dB/Hz，可以满足干涉测量光纤传感激光器的要求[30]。此外，图 9(e)的插图中给出了 0～200 kHz范围内分辨率带宽为 500 Hz 的相对强度噪声谱。在插图中可以观察到掺铥光纤激光器在 15.6 kHz 附近的松弛振荡频率峰值为−82.77 dB/Hz，同时还捕捉到了由外部干扰或测量系统产生的几个噪声峰值。

图 9 激光器的频率输出特性。(a) 0～100 MHz 范围内激光器的自零差射频频谱；(b) 0～500 MHz 范围内激光器的自零差射频频谱；(c) 0～1 GHz 范围内激光器的自零差射频频谱；(d)去除饱和吸收体后的激光射频频谱；(e)激光的相对强度噪声谱

Fig.9 Frequency output characteristics of the proposed laser. (a) Self-homodyne radio frequency (RF) spectrum of laser in 0–100 MHz; (b) self-homodyne RF spectrum of laser in 0–500 MHz; (c) self-homodyne RF spectrum of laser in 0–1 GHz; (d) RF spectrum of the main cavity without SA; (e) relative intensity noise (RIN) spectrum of the laser

为了进一步表征掺铥光纤激光器的线宽特性，采用基于 3×3 光纤耦合器的非平衡迈克耳孙干涉仪(MI)对激光器的频率噪声进行测量[30]，并结合 β-分割线法计算激光线宽。在激光线宽测量系统[31]中，用 50 m 长的标准单模光纤(SMF)代替传统延迟自外差线宽测量方法中的超长延迟线，以解决 2 μm 波段光传输损耗较大的问题。系统接收到的干涉条纹包含在迈克耳孙干涉仪延迟时间 τ 内积累的差分相位波动信息中，以此信息计算激光瞬时相位波动和频率波动的功

率谱密度(PSD)，计算结果如图 10(a)所示。随着测量时间延长，频率波动的功率谱密度中的 1/f 型噪声会引起线宽增加，从而在较短的测量时间下能够更好地反映线宽结果，因此选取测量时间为 0.001 s，此时激光器线宽约为 9.17 kHz[32-33]。

为了实现所提掺铥光纤激光器输出激光波长的可调谐特性，通过微位移平台/应力调节架拉伸光纤布拉格光栅，将光纤布拉格光栅固定在应力调节架的两端，通过调节位移的大小，实现波长从

2048.76 nm 到 2051.46 nm 的可调谐，可调谐范围约 2.7 nm，输出光谱如图 10(b)所示。由于本实验中的光纤光栅没有涂覆层，在拉伸状态下易断开，为了防止其损坏，没有继续拉伸增大其可调谐范围，但其可调谐范围可通过良好的涂覆材料和涂覆工艺进一步扩大。

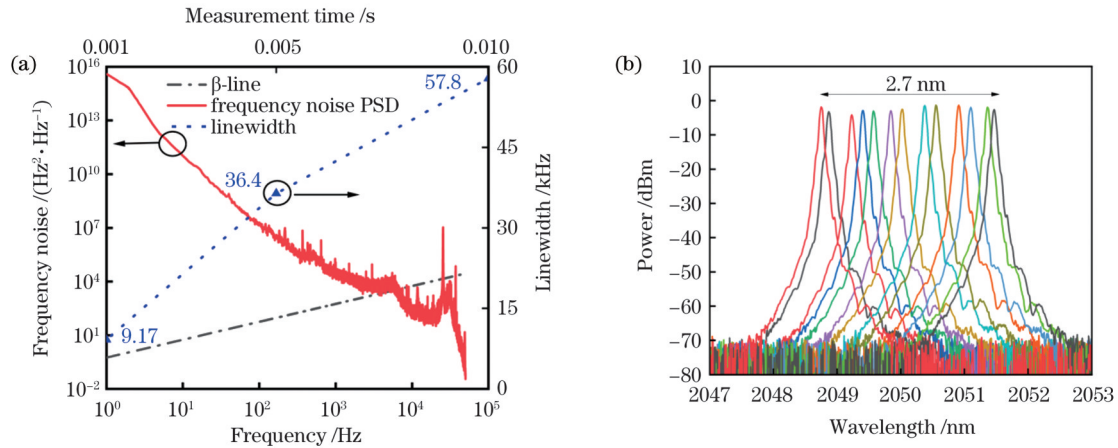图 10　激光器的输出线宽及可调谐性能。(a)激光器频率噪声的功率谱密度；(b)波长可调谐范围为 2.7 nm 的激光输出光谱

Fig. 10　Output line width and tunability of the proposed laser. (a) Power spectral density of frequency noise of the laser; (b) spectrum of the laser output with a wavelength-tunable range of 2.7 nm

最后，将该激光器的结构、性能指标与其他基于不同技术的单纵模掺铥光纤激光器进行对比，如表 1 所示。可以看出，本文所提激光器具有高光信噪比、高稳定性、窄线宽等优势。

表 1　基于不同技术的单纵模掺铥光纤激光器的性能指标比较

Table 1　Performance index comparison of SLM TDFL based on different techniques

Ref.	Wavelength /nm	Maximal power fluctuation /dB	Maximal wavelength drift /nm	Maximal OSNR / dB	Linewidth /kHz
[15]	1941.56	1.46	0.019	55.8	14.1
[19]	2048.3	0.641	0.01	62	
[22]	1941.6	1.5	0.04	32	
[32]	1940	0.26	0.01	60	8
This work	2048.76	0.15	0.02	68	9.17

4　结　　论

报道了一种工作在 2050 nm 波段的基于复合双环腔与饱和吸收体的单纵模窄线宽掺铥光纤激光器，并对其输出稳定性和线宽特性进行了详细表征。对所提滤波器的滤波性能进行了详细的理论分析，验证了该结构能够很好地抑制密集的多纵模并且具有易于制作、容差性强等优点。未泵浦的掺铥光纤具有优秀的单纵模选择能力，可保证激光器处在稳定的单纵模状态下。在室温条件下，所提激光器获得了中心波长为 2048.76 nm、光信噪比为 68 dB 的稳定输出，其最大波长漂移和功率波动分别为 0.02 nm 和 0.15 dB。激光器的频率噪声采用基于 3×3 光耦合器的激光器相位解调系统进行测量，输出激光的线宽值为 9.17 kHz。当频率高于 1 MHz 时，相对强度噪声低于−125.69 dB/Hz。所提激光器具有高光信噪比、高稳定性、窄线宽等优点，可通过降低熔接损耗、进行良好的隔振和温度补偿等措施实现性能更为优越的激光输出，从而更广泛地应用于激光雷达和空间光通信系统中。

参 考 文 献

[1] 孟佳，张伟，赵开祺，等. 国产化掺铥光纤激光振荡器性能研究[J]. 中国光学，2019，12(5): 1109-1117.
　　Meng J, Zhang W, Zhao K Q, et al. Performance of a homemade thulium-doped fiber laser oscillator[J]. Chinese Optics, 2019, 12 (5): 1109-1117.

[2] Scholle K, Lamrini S, Koopmann P, et al. 2 μm laser sources and their possible applications[M]//Frontiers in guided wave optics and optoelectronics. London: InTech, 2010.

[3] 赵桂娟，王雨雷，陈彬，等. LD 侧面泵浦被动调 Q 环形腔单纵模激光器[J]. 光学学报，2022，42(19): 1914003.
　　Zhao G J, Wang Y L, Chen B, et al. LD side-pumped passively Q-switched ring cavity single longitudinal-mode laser[J]. Acta Optica Sinica, 2022, 42(19): 1914003.

[4] 刘硕. 面向 2 μm 波段大功率光纤激光系统的高质量多波长及脉冲激光种子源研究[D]. 北京: 北京交通大学，2017: 20-28.
　　Liu S. Research on high-quality multi-wavelength and pulsed laser seed source for 2 μm band high-power fiber laser system[D]. Beijing: Beijing Jiaotong University, 2017: 20-28.

[5] Omiya T, Yoshida M, Nakazawa M. 400 Gbit/s 256 QAM-OFDM transmission over 720 km with a 14 bit/s/Hz spectral efficiency using high-resolution FDE[J]. Optics Express, 2013, 21(3): 2632-2641.

[6] Liu Y, Liu J Q, Chen W B. Eye-safe, single-frequency pulsed all-fiber laser for Doppler wind lidar[J]. Chinese Optics Letters, 2011, 9(9): 090604.

[7] Liu B, Jia C L, Zhang H, et al. DBR fiber laser-based active

temperature sensor and its applications in measurement of fiber birefringence[J]. Microwave and Optical Technology Letters, 2010, 52(1): 41-44.

[8] Geng J H, Spiegelberg C, Jiang S B. Narrow linewidth fiber laser for 100-km optical frequency domain reflectometry[J]. IEEE Photonics Technology Letters, 2005, 17(9): 1827-1829.

[9] 郭哲灿, 谢芳, 郭晓蕾, 等. 基于复合谐振腔的多波长窄线宽光纤激光器[J]. 激光与光电子学进展, 2022, 59(17): 1714008.
Guo Z C, Xie F, Guo X L, et al. Multiwavelength and narrowlinewidth fiber laser based on composite resonator[J]. Laser & Optoelectronics Progress, 2022, 59(17): 1714008.

[10] Katori H. Optical lattice clocks and quantum metrology[J]. Nature Photonics, 2011, 5(4): 203-210.

[11] Chou C W, Hume D B, Rosenband T, et al. Optical clocks and relativity[J]. Science, 2010, 329(5999): 1630-1633.

[12] Chen D, Fu H, Liu W. Single-longitudinal-mode erbium-doped fiber laser based on a fiber Bragg grating Fabry-Perot filter[J]. Laser Physics, 2007, 17(10): 1246-1248.

[13] Cheng Y, Kringlebotn J T, Loh W H, et al. Stable single-frequency traveling-wave fiber loop laser with integral saturable-absorber-based tracking narrow-band filter[J]. Optics Letters, 1995, 20(8): 875-877.

[14] Meng Z, Stewart G, Whitenett G. Stable single-mode operation of a narrow-linewidth, linearly polarized, erbium fiber ring laser using a saturable absorber[J]. Journal of Lightwave Technology, 2006, 24(5): 2179-2183.

[15] Bai Y, Yan F P, Feng T, et al. Demonstration of linewidth measurement based on phase noise analysis for a single-frequency fiber laser in the 2 μm band[J]. Laser Physics, 2019, 29(7): 075102.

[16] Feng T, Ding D L, Zhao Z W, et al. Switchable 10 nm-spaced dual-wavelength SLM fiber laser with subkHz linewidth and high OSNR using a novel multiple-ring configuration[J]. Laser Physics Letters, 2016, 13(10): 105104.

[17] Feng T, Jiang M L, Wei D, et al. Four-wavelength switchable SLM fiber laser with sub-kHz linewidth using superimposed high-birefringence FBG and dual-coupler ring-based compound cavity filter[J]. Optics Express, 2019, 27(25): 36662-36679.

[18] Feng T, Wei D, Bi W, et al. Wavelength-switchable ultra-narrow linewidth fiber laser enabled by a figure-8 compound-ring-cavity filter and polarization-managed four-channel filter[J]. Optics Express, 2021, 29(20): 31179-31200.

[19] Guo Y, Yan F P, Feng T, et al. Wavelength-switchable single-longitudinal-mode thulium-doped fiber laser at 2.05 μm using a superimposed fiber Bragg grating[J]. Infrared Physics and Technology, 2022, 122: 104058.

[20] Han W G, Yan F P, et al. Wavelength-switchable single-longitudinal-mode thulium-doped fiber laser with sampled fiber Bragg gratings[J]. IEEE Access, 2021, 9: 62212-62218.

[21] Li Q, Yan F P, Peng W J, et al. Single-frequency ring-cavity Tm-doped fiber laser based on CMFBG filter[J]. Laser Physics Letters, 2013, 10(9): 095105.

[22] 白燕, 延凤平, 孙景辉, 等. 基于 F-P 滤波器和饱和吸收体的单纵模掺铥激光器[J]. 科技导报, 2016, 34(16): 104-107.
Bai Y, Yan F P, Sun J H, et al. Single-longitudinal-mode thulium-doped fiber laser using Fabry-Perot filter and saturable absorber[J]. Science & Technology Review, 2016, 34(16): 104-107.

[23] 白燕, 延凤平, 冯亭, 等. 基于保偏掺铥光纤饱和吸收体的 2 μm 波段超窄线宽光纤激光器[J]. 中国激光, 2019, 46(1): 0101003.
Bai Y, Yan F P, Feng T, et al. Ultra-narrow-linewidth fiber laser in 2 μm band using saturable absorber based on PM-TDF[J]. Chinese Journal of Lasers, 2019, 46(1): 0101003.

[24] Feng S, Mao Q, Tian Y et al. Widely tunable single longitudinal-mode fiber laser with a cascaded fiber ring secondary cavity[J]. IEEE Photonics Technology Letters, 2013, 25(4): 323-326.

[25] Zhang L N, Yan F P, Feng T, et al. Six-wavelength-switchable narrow-linewidth thulium-doped fiber laser with a polarization-maintaining sampled fiber Bragg grating[J]. Optics and Laser Technology, 2021, 136: 106788.

[26] Guo B, Guo X Y, Tang L G, et al. Ultralong-period grating-based multiwavelength ultrafast fiber laser[J]. Chinese Optics Letters 2021, 19(7): 071405.

[27] Feng T, Ding D L, Yan F P, et al. Widely tunable single-/ dual-wavelength fiber lasers with ultra-narrow linewidths and high OSNR using a high-quality passive subring cavity and novel tuning method[J]. Optics Express, 2016, 24(17): 19760-19768.

[28] Cheng D, Yan F P, Feng T, et al. A six-wavelength-switchable SLM thulium-doped fiber laser was enabled by the sampled FBGs and a 3 × 3 coupler-based dual-ring compound cavity filter[J]. IEEE Photonics Journal 2022, 14(2): 1515908.

[29] Wang Z K, Shang J M, Mu K L, et al. A single-longitudinal-mode fiber laser with ultra-narrow linewidth and extremely high stability was obtained using a triple-ring passive substrate resonator [J]. Optics and Laser Technology, 2020, 130: 106329.

[30] Cranch G A. Frequency noise reduction in erbium-doped fiber distributed-feedback lasers by electronic feedback[J]. Optics Letters, 2002, 27(13): 1114-1116.

[31] Zhang J L, Yue C Y, Schinn G W, et al. Stable single-mode compound-ring erbium-doped fiber laser[J]. Journal of Lightwave Technology, 1996, 14(1): 104-109.

[32] Xu D, Yang F, Chen D J, et al. Laser phase and frequency noise measurements were performed using a Michelson interferometer composed of a 3×3 optical fiber coupler[J]. Optics Express, 2015, 23(17): 22386-22393.

[33] 王雪, 延凤平, 韩文国. 基于特殊子环腔单纵模窄线宽掺铥光纤激光器[J]. 中国激光, 2019, 46(9): 0901001.
Wang X, Yan F P, Han W G. Single longitudinal mode narrow linewidth thulium-doped fiber laser with special subring cavity[J]. Chinese Journal of Lasers, 2019, 46(9): 0901001.

Single Longitudinal Mode Narrow Linewidth Thulium-Doped Fiber Laser Based on Compound Double-Ring Cavity and Saturable Absorber

Gao Jiao[1], Yan Fengping[1*], Feng Ting[2], Yang Dandan[1], Li Ting[1], Qin qi[1], Guo Hao[1], Tan Haoyu[1], Li Guangbo[1]

[1]School of Electronic and Information Engineering, Beijing Jiaotong University, Beijing 100044, China;
[2]Photonics Information Innovation Center, College of Physics Science & Technology, Hebei University, Baoding 071002, Hebei, China

Abstract

Objective In recent years, the development of thulium-doped fiber lasers (TDFL) gradually followed the footsteps of ytterbium-

doped and erbium-doped fiber lasers. The tunable range of TDFL is 1400–2200 nm, covering the atmospheric transmission window. In this window, the allowed power transmission of light in free space can be several orders of magnitude higher than that of the other wavelength bands. In particular, optical power transmission exceeds 80% in the 2050 nm wavelength band, making it possible to use TDFL in this band for free-space optical communications and atmospheric Doppler lidar. The TDFL operating wavelength is in the 2 μm band, which is a safe operating band for human eyes, and in which there is a high transmittance atmospheric window and strong absorption peaks of multiple gas molecules and OH^- ions. Therefore, lasers in this band are favored by various application industries, especially in the free-space optical communication field, where human eye safety is a requirement. Single longitudinal mode (SLM) fiber lasers have excellent characteristics, such as high beam quality, good coherence, and narrow linewidth, and are widely used as the preferred light source in multiple important fields. For example, fiber lasers with a narrow linewidth output have been used in ultra-long-range coherent optical communication, fiber optic sensing, optical metrology, high-resolution spectroscopy, and lidar, and have potential applications in optical atomic clocks, fundamental constant measurements, and physics. Therefore, the realization of a stable single longitudinal-mode narrow-linewidth laser source in the 2050 nm band is indispensable.

Methods　The proposed structure predominantly consists of a ring main cavity and a compound sub-cavity (Fig. 1). The 793 nm pumped source output is input into the ring cavity through the fiber combiner, a 4 m long double-clad thulium-doped fiber is used as the gain medium, and the circulator ensures unidirectional transmission of light inside the ring cavity. A 0.5 m length of unpumped thulium-doped fiber is added to port 2 of the ring as the saturable absorber (SA), making it equivalent to a dynamic self-tracking narrow-band filter, which effectively suppresses the multi-longitudinal mode oscillation, realizing single longitudinal mode operation and compressing the narrow linewidth. A fiber Bragg grating (FBG) is used as a wavelength-selective device. The optical signal reflected by the FBG is injected into a composite double-loop cavity composed of three couplers and a composite double-loop cavity structure (Fig. 3), which consists of one 3×3 coupler OC1 and two 2×2 couplers OC2 and OC3 which are connected in sequence. The 3×3 coupler OC1 has a 33∶33∶33 output and divides the input optical signal into three optical signals. The coupling ratio of both 2×2 couplers is 20∶80. The output laser is generated from the 10% port of the 90∶10 coupler.

Results and Discussions　The laser was developed and tested on an ultrastable optical stage at room temperature. A stable laser output was obtained when the pumping power reached 4 W. The central wavelength was 2048.76 nm, and the optical signal-to-noise ratio was 68 dB. The output spectrum was measured every 6 min for 60 min, and the spectrum obtained after ten consecutive scans [Fig. 8(a)]. To further quantify the stability of the laser, the power jitter and wavelength drift results over 60 min were analyzed with power fluctuation less than 0.15 dB and wavelength drift less than 0.02 nm [Fig. 8(b)], indicating that the laser had good output stability at room temperature. The results of the single longitudinal mode of the output laser using the self-homodyne method show no obvious mode-hopping phenomenon over the three measurement ranges (Fig. 9). To demonstrate the stability of the laser's single longitudinal mode, ten sets of measurements were performed within 60 min, and no beat frequency signal generated by the longitudinal mode was captured [Fig. 9(a) inset]. When the SA was removed, a nonzero frequency rate peak was observed in the 0–500 MHz measurement range [Fig. 9(d)]. The results show that the composite double-ring cavity effectively suppresses most longitudinal modes in the cavity; however, the remaining longitudinal modes must be further suppressed using saturable absorbers. To further characterize the linewidth characteristics of the TDFL, the frequency noise of the laser was measured using an unbalanced Michelson interferometer based on a 3×3 fiber coupler, and the linewidth of the laser was calculated using the β-separation line method. The laser linewidth was 9.17 kHz at 0.001 s and the relative intensity noise is below -129.69 dB/Hz at frequencies above 1 MHz.

Conclusions　A single longitudinal mode narrow linewidth TDFL based on a compound double-ring cavity with a saturable absorber operating in the 2050 nm wavelength band is reported, with its output stability and linewidth characteristics characterized in detail. The performance of the proposed filter was analyzed in detail, and it was confirmed that the structure suppresses dense multilongitudinal modes well and has the advantages of simple fabrication and high tolerance. In combination with the excellent single longitudinal mode selection capability of the unpumped thulium-doped fiber, the laser was guaranteed to be in a stable single longitudinal mode state. Experimental results demonstrate that the proposed laser has the advantages of a high optical signal-to-noise ratio (OSNR), high stability, and narrow linewidth, and can be more widely used in lidar and space optical communication systems by reducing fusion loss, good vibration isolation, and temperature compensation to achieve a superior laser output.

Key words　lasers; thulium-doped fiber laser; single longitudinal mode; sub-ring cavity; saturable absorber